Research Article | Vol. 32, No. 12 / 3 Jun 2024 / Optics Express 20976
Optics EXPRESS

Pre-distortion adaptive optics for optical feeder links: simulations and performance analyses

ILIJA R. HRISTOVSKI,[1,2,*] JAMES OSBORN,[3] OLLIE J. D. FARLEY,[3] MATTHEW J. TOWNSON,[4] RAMON MATA CALVO,[5] BRUNO FEMENÍA-CASTELLA,[1] JOANA S. TORRES,[1] JONATHAN F. HOLZMAN,[2] AND ANDREW P. REEVES[1]

[1]German Aerospace Center, Münchener Str. 20, 82234 Weßling, Germany
[2]School of Engineering, The University of British Columbia, 1137 Alumni Ave., Kelowna, British Columbia, V1 V 1V7, Canada
[3]Durham University, Department of Physics, Centre for Advanced Instrumentation, Lower Mountjoy, South Rd., Durham, DH1 3LE, UK
[4]Northumbria University, Dept. Math, Physics, and Electrical Engineering, Ellison Pl., Newcastle upon Tyne, NE1 8ST, UK
[5]ESTEC, European Space Agency, Keplerlaan 1, 2201 AZ Noordwijk, Netherlands
[*]ilija.hristovski@dlr.de

Abstract: Optical feeder links offer immense utility in meeting future communication demands—however, atmospheric turbulence limits their performance. This work targets this challenge through analyses of a bidirectional free-space optical communication (FSOC) link that incorporates pre-distortion adaptive optics (AO) between the next-generation optical ground station at the German Aerospace Center (DLR) Oberpfaffenhofen and the laser communications terminal on Alphasat—a satellite in geostationary orbit (GEO). The analyses are performed via end-to-end Monte Carlo simulations that provide realistic performance estimates of the bidirectional FSOC link for a GEO feeder link scenario. We find that applying pre-distortion AO reduces the total uplink losses of the bidirectional FSOC link by up to 10 dB and lessens the scintillation at the GEO satellite by an order of magnitude. Moreover, applying pre-distortion AO eases the link budget requirements needed for maintaining 99.9% link uptime by as much as 20-40 dB, while its use with a laser guide star shows an additional performance improvement of up to 8 dB. These findings demonstrate the desirability and feasibility of utilizing pre-distortion AO for the realization of optical feeder links.

1. Introduction

The field of free-space optical communication (FSOC) has shown rapid growth—due in large part to increasing demands for high communication data rates and worldwide coverage [1,2]. Immense bandwidth, improved security, and an unlicensed spectrum are some of the key advantages of FSOC-based technologies that are driving this growth [3]. Of particular interest are FSOC links that transmit data from an optical ground station (OGS) to an orbiting satellite, via laser beam, and then distribute this data to various geographical regions on Earth. Such links can be used in isolation, to enable high-speed and secure connectivity to regions where traditional communication networks are infeasible or nonexistent [1], or merged with radio frequency communication links, for distribution across urban centers via so-called optical feeder links [4]. One desirable configuration for optical feeder links involves an OGS feeding data via a bidirectional FSOC link to a single satellite in geostationary orbit (GEO), which then distributes

#521494 https://doi.org/10.1364/OE.521494
Journal © 2024 Received 15 Feb 2024; revised 22 Apr 2024; accepted 10 May 2024; published 22 May 2024

Optics EXPRESS

this data to multiple Earth-based transceivers using radio frequency communication links. This is known as a GEO feeder link [5–7]. Here, the bidirectional FSOC link consists of a downlink laser beam that is transmitted from the GEO satellite, and is typically used as a reference beacon for tracking by the OGS, and an uplink laser beam that carries data from the OGS to the GEO satellite for distribution. Such GEO feeder links offer significant benefits due to the high altitude and wide field-of-view of the GEO satellite, which enables uninterrupted coverage spanning continental scales [8], and the tremendous data rates of FSOC technology, at terabit-per-second levels [5,9,10].

Despite the many advantages of GEO feeder links, one long-standing challenge is their bidirectional FSOC link's susceptibility to atmospheric turbulence [11,12]. In essence, turbulence-induced fluctuations in the atmosphere's refractive index impart wavefront distortions onto the propagating laser beams, which leads to beam wander (i.e., shifts in the beam's direction) and scintillation (i.e., intensity fluctuations at the receiver due to the interference of subsequent wavefronts). Such effects yield increased fading (or power fluctuations) at the receiver, reduced bandwidth, and corrupted data, which ultimately limits the link performance [12,13]. Fortunately, adaptive optics (AO) systems show promise in mitigating these turbulence-induced fluctuations and restoring link performance [14–17].

While AO systems have traditionally been used in astronomical applications, they have witnessed growing interest for FSOC links. One emerging concept employs pre-distortion AO within the bidirectional FSOC link for a GEO feeder link configuration [17]. In such links, the downlink laser beam sent from the GEO satellite to the OGS is subjected to wavefront distortions, from atmospheric turbulence, and an AO system in the OGS corrects these distortions in (near) real-time by applying the conjugate of the wavefront distortions via actuated optics. Concurrently, these conjugate distortions are applied to the uplink laser beam's wavefronts to "pre-distort" the beam. As the uplink laser beam then propagates through the atmosphere, its wavefront pre-distortion is counteracted by the atmospheric turbulence, leaving a "corrected" beam propagating to the GEO satellite. In this way, pre-distortion AO has the potential to mitigate the effects of atmospheric turbulence on the downlink and uplink laser beams, making it an enabling technology for the realization of GEO feeder links.

The concept of pre-distortion AO, as applied to GEO feeder links, has been drawing attention in recent years [17–20]. Osborn *et al.* [17] explored pre-distortion (also termed pre-compensation) AO, via idealized simulations, to provide an upper limit on the proposed benefits of implementing pre-distortion AO in a bidirectional FSOC link. However, their work did not account for some of the prominent errors that could be expected in real-world implementations.

Given the significant benefits of GEO feeder links and the advantages of pre-distortion AO, we provide detailed analyses in this work on the performance of bidirectional FSOC links employing pre-distortion AO. This is done for a real-world GEO feeder link scenario using realistic Monte Carlo end-to-end simulations configured for bidirectional FSOC links between the next-generation OGS at the German Aerospace Center (DLR) Oberpfaffenhofen and the GEO satellite Alphasat. The bidirectional FSOC links and AO system that enable them are configured according to the real AO system in DLR's OGS and its ability to establish links with Alphasat. The configuration and simulation are described in section 2. The relevant error sources incorporated into the simulation, thus making it represent the real-world pre-distortion AO system within DLR's next-generation OGS, are characterized in section 3, with insight given on relevant theoretical models. The AO configurations are described in section 4, and the performance metrics used to characterize the system's performance are described in section 5. The performance analyses and subsequent discussions are presented in section 6. Concluding remarks on our work and its potential for use in GEO feeder links are presented in section 7.

Optics EXPRESS

2. End-to-end AO simulation configuration

End-to-end Monte Carlo simulations are used in this work to evaluate a bidirectional FSOC link and the pre-distortion AO system that enables it for a GEO feeder link scenario. The envisioned bidirectional FSOC link is depicted on the left in Fig. 1 and the pre-distortion AO system is depicted on the right.

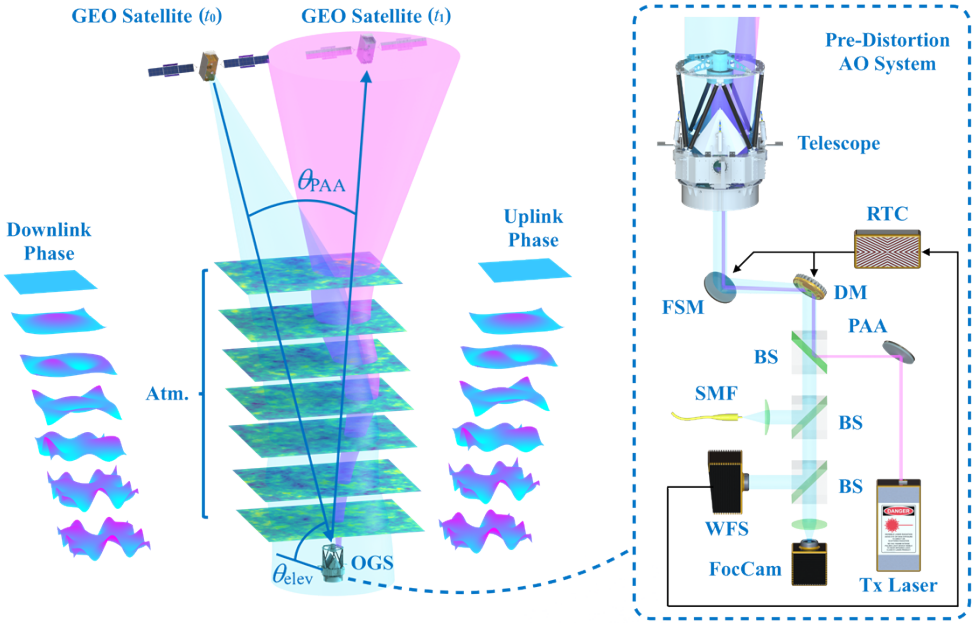

Fig. 1. Representative depiction of the bidirectional FSOC link for a GEO feeder link scenario (left) and the pre-distortion AO system that enables it (right). On the left, the downlink laser beam (blue) propagates from the GEO satellite, through the atmosphere (Atm), to the OGS at time t_0, while the pre-distorted uplink laser beam (pink) is launched from the OGS and propagates at a point-ahead angle, θ_{PAA}, and elevation angle, θ_{elev}, to the future position of the GEO satellite at time t_1. The phase profiles of each laser beam are tracked to show the imparting or correction of turbulence-induced distortions on each beam. On the right, an exploded view is shown of the pre-distortion AO system that corrects the downlink laser beam and pre-distorts the uplink laser beam. The pre-distortion AO system includes a telescope, a fast-steering mirror (FSM), a deformable mirror (DM), a single-mode fiber (SMF), a wavefront sensor (WFS), a focus camera (FocCam), a point-ahead angle mirror (PAA), a real-time control computer (RTC), multiple beam splitters (BS), and an uplink laser (Tx Laser).

The simulation begins at time t_0 with a plane wave at the top of the atmosphere propagating along the downlink direction, as it is assumed that the downlink laser beam has diverged sufficiently from the GEO satellite to the upper atmosphere. The wavefront of this downlink laser beam (shown in blue in Fig. 1) is distorted as it passes through the atmosphere, which is represented in the simulation by seven atmospheric phase screens. The phase screens follow *von Kármán* turbulence statistics [21,22], with each having a defined altitude, turbulence strength, wind speed, and wind direction. Angular spectrum propagation (employing a specialized solution to the Fresnel diffraction integral) [23] is used to simulate the propagation and diffractive effects between each atmospheric layer. A fraction of the downlink laser beam is then received by the telescope within the OGS, and the distortions imparted onto this beam by the atmosphere are eventually measured by a Shack-Hartmann wavefront sensor (WFS). As the downlink laser beam

Optics EXPRESS

is actually propagated to the WFS' sensor plane, diffractive and scintillation effects are measured by the WFS. A focus camera is also simulated to observe the corrected point spread function and therefore understand the quality of the AO correction.

The turbulence-induced wavefront distortions imparted onto the downlink laser beam are corrected at the OGS by a fast-steering mirror (FSM) and deformable mirror (DM), which apply the conjugate of the received phase of the laser beam. Namely, the FSM corrects for the low-order distortions (thus reducing the aforementioned beam wander) while the DM compensates for the high-order distortions (thus reducing the scintillation effects). A control system that runs a standard integrator controller via a real-time control computer computes the corrective commands that are applied to the FSM and DM according to the WFS measurements. Ultimately, the applied correction and reduced distortions on the downlink laser beam improve the instantaneous and long-term point spread function observed on the focus camera, as quantified by the Strehl ratio, and increase the light coupled into the receiver's single-mode optical fibre, for improved communication performance.

An uplink laser beam (shown in pink in Fig. 1) is launched from the OGS to the GEO satellite via the same FSM and DM, thus "pre-distorting" the uplink laser beam. It is important to note here that this uplink laser beam is also launched with an angular offset from the downlink laser beam, called the point-ahead angle. The point-ahead angle directs the uplink laser beam in front of the GEO satellite's current observed position, to have the beam arrive at the GEO satellite's future position (given the beam's transit time and the satellite's motion). As such, the uplink laser beam propagates to the top of the atmosphere, where it arrives with minimal wavefront distortion, and onward to the GEO satellite, according to far-field (Fraunhofer) propagation. The latter propagation (at time t_1) is incorporated into our simulation by way of a fast-Fourier transform.

Given this link configuration, the relative loss at the satellite (measured in dB) is determined by calculating the contribution of the uplink laser beam's power entering the satellite's aperture, as compared to the total power available at GEO. Static losses (due to the uplink transmitter/receiver efficiency and atmospheric attenuation) are added to this relative loss at the satellite to give the total (uplink) loss.

Figure 2 summarizes the above scenario and outlines the 15 steps taken during each iteration of the simulation.

It should be noted that the storage buffer mentioned in step 5 is used to simulate the temporal delay that results from the lag between when a measurement is made by the WFS and when a correction by the FSM and DM is applied. This is further described in section 3.

An important aspect to consider for the bidirectional FSOC link is the point-ahead angle, which is approximately 18 µrad, or 4 arcseconds, for a satellite in GEO [4,20]. In the case that the downlink laser beam is used as a reference beacon to measure the atmospheric distortions, this angular offset between the downlink and uplink laser beams implies that the atmospheric distortions imparted onto the laser beams become partly spatially decorrelated with increasing altitude and large point-ahead angles—an effect that is amplified in stronger atmospheric turbulence and is known as angular anisoplanatism [24]. The implications of this angular anisoplanatism will be discussed later in this work. The point-ahead angle is incorporated into the simulation as described in step 2 of Fig. 2. In essence, smaller phase screens are extracted from the larger atmospheric phase screens and along the downlink and uplink lines-of-site, such that an 18-µrad point-ahead angle subtends between the downlink and uplink laser beams.

The relevant simulation parameters are listed in Table 1. The simulation represents the bidirectional FSOC link between DLR's next-generation OGS, with its installed AO system, and the GEO satellite Alphasat, with its 1064-nm laser communication terminal [25]. The link distance is approximately 38824.7 km.

The Hufnagel-Valley 5/7 profile is employed in this work to represent the vertical distribution of atmospheric turbulence strengths, as this profile is commonly used when simulating AO

Optics EXPRESS

Table 1. Simulation Parameters

Parameter	Unit	Value	Variable
Link Parameters			
Wavelength	nm	1064	λ
Elevation angle	deg	33	θ_{elev}
Point-ahead angle	μrad	0, 18	θ_{PAA}
OGS Parameters			
Downlink telescope diam.	cm	80	D_{Rx}
Downlink central obs. diam.	cm	30	D_{cent}
Uplink hard aperture diam.	cm	25	D_{Tx}
Uplink beam waist	cm	~8.8	ω_0
OGS configuration	–	Monostatic	–
Satellite Parameters			
Satellite aperture diameter	mm	135	D_{SAT}
Link distance	km	38824.7	L
General Parameters			
Control system type	–	Integrator	–
AO loop iteration rate	kHz	2	f_{Loop}
AO loop time-step	ms	0.5	τ_{Loop}
Loop delay	frames	2	–
WFS Parameters			
Number of subapertures	–	116 (arranged in 13×13 circle)	N_{subaps}
Read noise	e-	120	n_{read}
Shot noise	–	Poisson Statistics	n_{shot}
Incident power on AO system	μW	2	P_{AO}
Corrector Parameters			
Corrector types	–	Tip/Tilt FSM and Zonal DM	–
Number of DM actuators	–	184 (16×16 arranged in a circle and actuated with only 14×14 illuminated)	N_{acts}
Atmospheric Parameters			
Number of phase screens	–	7	–
Layer altitudes (Zenith)	m	[198, 5188, 9050, 12321, 15707, 19165, 22662]	h
Layer wind speeds	m/s	[5.8, 18.9, 34.9, 25.7, 10.3, 5.5, 5.0]	$V(h)$
Layer wind directions	deg	[0, 90, 180, 270, 0, 90, 180]	ϕ
Profile Fried parameters (Zenith and 500 nm)	cm	[1.44, 1.94, 2.44, 3.54, 4.97]	r_0
Profile Greenwood Frequencies	Hz	[92.6, 72.1, 60.2, 46.5, 38.6]	f_{G}
Fractional layer turbulence strengths	%	$\left\{ \begin{bmatrix} 99.0, 0.275, 0.314, 0.253, 0.093, 0.021, 0.003 \\ 98.4, 0.449, 0.513, 0.413, 0.152, 0.034, 0.005 \\ 97.7, 0.657, 0.751, 0.605, 0.223, 0.049, 0.008 \end{bmatrix} \begin{bmatrix} 95.7, 1.23, 1.40, 1.13, 0.416, 0.092, 0.014 \\ 92.5, 2.15, 2.46, 1.98, 0.732, 0.162, 0.025 \end{bmatrix} \right\}$	$\text{Cn}^2(h)$

Optics EXPRESS

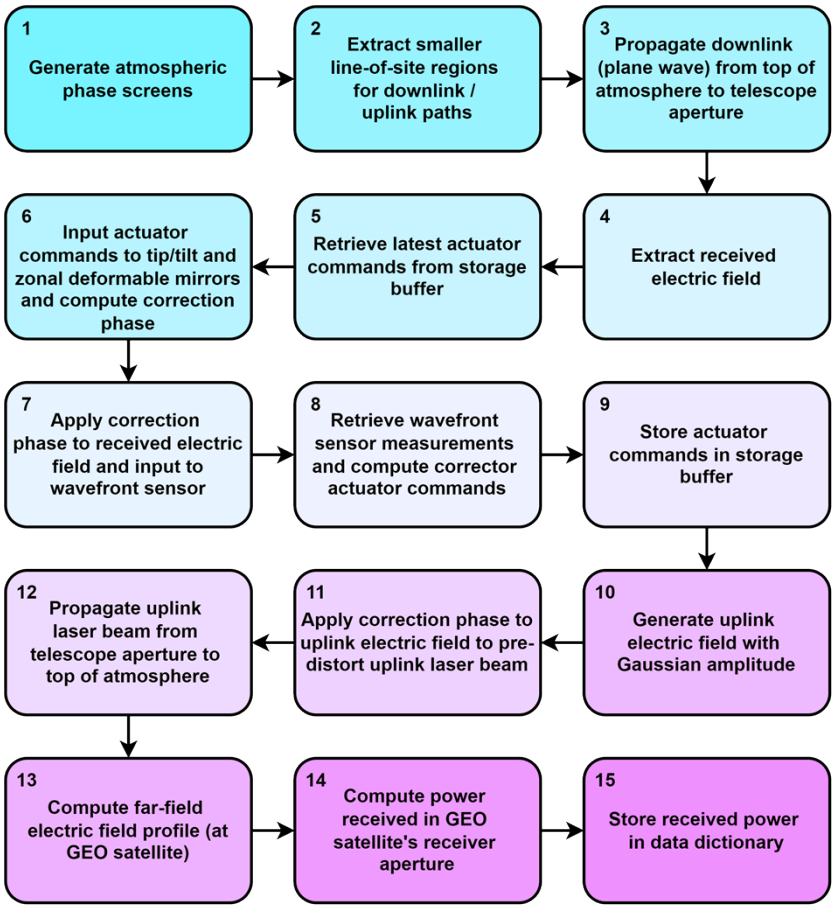

Fig. 2. Flow chart of the simulation that describes the 15 steps taken during each iteration.

systems in FSOC and it provides a good basis for comparison of performance among different systems. More specifically, five variations of a modified Hufnagel-Valley 5/7 profile are employed in our simulation to synthesize atmospheres that range from exhibiting "weak'' turbulence (being representative of nighttime operation) to "strong'' turbulence (being representative of daytime operation). These profiles lead to five subsequent spatial coherence lengths, known as Fried parameters, r_0, which range from approximately 1.4–5 cm (at zenith and a wavelength of 500 nm) or 3.6–12.3 cm (at zenith and a wavelength of 1064 nm). The Bufton wind model [26] is also inherited by the atmospheric layers to represent the vertical distribution of transverse wind speeds. The atmospheric profiles used in this work follow those presented in Osborn *et al.* [17], which were made using the equivalent layers method [27], as this method ensures that the isoplanatic angle is preserved when discretizing atmospheric models. Despite the Hufnagel-Valley 5/7 profile being used in this work, as atmospheric turbulence profiling instruments and techniques become more developed and widely used [28,29], such tools and techniques will be useful in characterizing future OGS sites [30].

Optics EXPRESS

3. Theoretical analyses and sources of loss

3.1. Adaptive optics (AO) error sources

The performance estimates provided in this work are considered to be realistic and representative of a real-world bidirectional FSOC link applied to a GEO feeder link scenario, as they incorporate fundamental sources of error that manifest within DLR's actual AO system. While these error sources are listed below and are accurately represented within the simulation, it should be noted that the analytically calculated results that stem from these error sources (and are plotted as various lines in section 6) are shown for comparison with the simulated results, however, no analytically calculated errors are input into the end-to-end simulations. The sources of error are described as follows:

Temporal error manifests when the atmosphere's Greenwood frequency (or characteristic frequency) exceeds the correction bandwidth of the AO control loop. This error can be modelled according to Eq. 9.53 in Hardy [24] and incorporated into the simulation by way of a two-frame delay, meaning that the corrective commands applied to the FSM and DM at frame N_0 are based upon WFS measurements from frame N_{-2}. For our system, the AO correction bandwidth is roughly one-eighth of the AO loop iteration rate, i.e., 2000Hz / 8 $\approx$ 250 Hz. As this bandwidth is larger than the Greenwood frequency values for the five atmospheric profiles listed in Table 1, temporal error should have minimal impact on the total wavefront error.

Fitting error manifests from the finite resolution of the DM and its resulting inability to perfectly correct for the increasingly fine structure of turbulent phase distortions. This error can be modelled from Eq. 3.1 in Tyson [31], or equivalently Eq. 27 from Hudgin [32], with the actuator constant, κ, being 0.30 rad^2 for our work. This error source is incorporated into our analyses via the simulation of a continuous faceplate DM that is deformed by zonal actuators, thus corroborating the value chosen for κ.

Anisoplanatic error manifests from the differing downlink and uplink laser beam paths through the atmosphere. The differing beam paths lead to growing spatial separation (and thus decorrelation) between the beams with increasing altitude. This error source can be modelled from Eq. 7 in Clénet *et al.* [33], whereby a modal analysis yields an expression for the residual anisoplanatic wavefront error from the covariance of the various Zernike expansion coefficients (defined for the lines of site separated by the point-ahead angle). This method was pioneered by Chassat [34] and expanded by Lognoné *et al.* [35].

Shack-Hartmann WFS measurement error manifests from a Shack-Hartmann type WFS's limitations on measuring subaperture tilt. This error can be modelled from Eq. 3.8 in Tyson [31], with SNR values having been taken from the simulation output as 1.5 (in strong turbulence conditions) to 4.5 (in weak turbulence conditions). This error source is incorporated into our analyses via the simulation of a Shack-Hartmann type WFS with the read and shot noise characteristics stated in Table 1.

Given the above sources of error, a theoretical AO error budget can be defined for the simulated AO system. The budget is illustrated in Fig. 3 as a plot of the mean squared wavefront error versus Fried parameter, r_0. It is clear from the results that fitting error rapidly becomes the dominant contribution to the total wavefront error in stronger turbulence conditions, i.e., smaller values of r_0.

3.2. Theoretical laser beam propagation and static losses

Andrews and Phillips [11] have developed a variety of expressions for atmospheric laser beam propagation, and these expressions are clearly summarized in Andrews *et al.* [36]. Of note in this latter work are Eqs. 24-26, which build upon the extended Maréchal approximation [37–40] to model the Strehl ratio and intensity of an uncorrected uplink laser beam at a satellite. These expressions were used in this work to model our fourth configuration, in section 4, which does

Optics EXPRESS

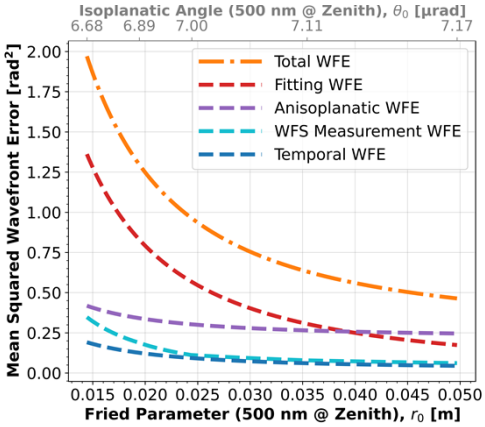

Fig. 3. Theoretical AO error budget depicting the various contributions from temporal, fitting, anisoplanatic, and Shack-Hartmann WFS measurement wavefront error (WFE) to the total mean squared WFE, as a function of the Fried parameter, r_0, on the lower horizontal axis and isoplanatic angle, θ_0, on the upper horizontal axis. The Fried parameter values span the appropriate range corresponding to the turbulence profiles described in Table 1.

not apply pre-distortion AO to the uplink laser beam. Another expression, namely Eq. 27 from Andrews *et al.* [36], models the Strehl ratio and intensity of a tilt-corrected uplink laser beam at a satellite. This expression was used in this work to model our third configuration, in section 4, which applies only tip-tilt pre-distortion AO over the transmitter launch sub-pupil.

Three static losses (listed in Table 2) are added to the relative loss measured at the GEO satellite. The uplink transmitter efficiency was measured, at 1064 nm, for DLR's next-generation OGS. The uplink receiver efficiency and losses due to atmospheric attenuation and/or clouds were taken from prior DLR studies that assessed various link budgets for GEO feeder links [6,10].

Table 2. Static Losses

Static Losses	
Uplink Transmitter Efficiency	-3.55 dB
Uplink Receiver Efficiency	-3.0 dB
Atmospheric Attenuation / Clouds	-2.0 dB

4. Simulated AO configurations

Multiple pre-distortion AO configurations were simulated within this work to demonstrate their potential link budget and stability improvements for the bidirectional FSOC link. The AO configurations are as follows:

i. **Idealized WFS/FSM/DM, high-order pre-distortion** (*Ideal WFS/FSM/DM + HOPD*)**:** This configuration assumes an ideal WFS, FSM, and DM, meaning that the received phase at the OGS is perfectly conjugated (to within the resolution of the simulation) and directly applied to pre-distort the uplink laser beam. Therefore, these results depict an upper limit for the improvements due to the application of pre-distortion AO. Temporal error is still included within this scenario due to the aforementioned two-frame delay. This AO configuration is representative of the AO system used in Osborn *et al.* [17].

Optics EXPRESS

ii. **Realistic WFS/FSM/DM, high-order pre-distortion** (*Real WFS/FSM/DM + HOPD*)**:** This configuration employs a realistic WFS (by way of a diffractive model that includes scintillation effects), FSM, and DM. The FSM is simulated as a tip-tilt mirror and the DM is simulated as a zonally-actuated continuous faceplate mirror. Temporal, fitting, and Shack-Hartmann WFS measurement errors are present in this scenario due to the two-frame delay, finite correction resolution of the DM, and noise and scintillation effects on the WFS.

iii. **Realistic WFS/FSM, tip/tilt pre-distortion** (*Real WFS/FSM + TTPD*)**:** This configuration employs a realistic WFS and FSM. It specifically measures (and then corrects / pre-distorts) the tip and tilt components manifesting only over the sub-pupil of the OGS telescope that the uplink laser beam is launched from. The received phase is masked to only allow the light over this transmitter launch sub-pupil to reach the WFS. This scenario can be theoretically modelled using Eq. 27 from Andrews *et al.* [36]. Temporal and Shack-Hartmann WFS measurement errors are also included in this scenario.

iv. **No pre-distortion** (*No PD*)**:** This configuration does not employ pre-distortion AO. The uplink laser beam is generated with a gaussian amplitude profile, as is done with all of the above scenarios, and a flat phase profile. It is then launched through the atmosphere and received at the GEO satellite. This scenario can be theoretically modelled using Eqs. 24-26 from Andrews *et al.* [36].

Two sub-configurations were also simulated for the first three configurations above to further investigate the effects of anisoplanatism due to the point-ahead angle. This analysis is crucial for bidirectional FSOC links that employ pre-distortion AO because a reference source of light is needed to probe the atmosphere and deduce the distortions imparted onto the propagating laser beam. The two sub-configurations are described as follows:

a. **"Perfect" laser guide star downlink reference** (*"Perfect" LGS DL Ref*)**:** This sub-configuration assumes that an ideal laser guide star is launched in the direction of the uplink laser beam and used as the downlink reference source of light (such that the distortions that will be imparted onto the uplink laser beam are measured by the WFS). No laser guide star dynamics are simulated in this scenario as the best-case performance when incorporating a laser guide star is desired. This scenario is also representative of operation with no point-ahead angle.

b. **Satellite downlink reference** (*Satellite DL Ref*)**:** This sub-configuration uses the downlink laser beam from the GEO satellite as the reference light source such that the atmospheric distortions that are imparted onto the uplink laser beam become increasingly decorrelated with the distortions imparted onto this downlink laser beam, with increasing altitude. This scenario inherits an 18 μrad point-ahead angle between the downlink and uplink laser beams, as this is representative of the point-ahead angle for the bidirectional FSOC link between DLR's next generation OGS and the GEO satellite Alphasat.

5. Uplink performance metrics

The end-to-end AO simulation employed in this work returns a two-dimensional electric field distribution at the plane of the GEO satellite. A fast-Fourier transform is used to represent far-field (Fraunhofer) propagation from the top of the atmosphere to the GEO satellite, such that the simulated grid resolution at the satellite is approximately 10 m. While recognizing that the GEO satellite's receiver diameter is 135 mm, the received power vector at the satellite, P, is calculated by scaling the intensity of the central pixel at GEO with the satellite's receiver aperture

Optics EXPRESS

for each iteration of the simulation. This approach is possible as there is little observed variation in the intensity profile at such spatial scales at the satellite. Such an approach also assumes that errors due to imperfect tracking of the GEO satellite by the OGS are negligible. Beam wander effects at the satellite are, however, still present when appropriate. Given these definitions, the following three uplink metrics were chosen:

Total (uplink) loss: The main component of this metric results from the ratio of power received at the GEO satellite to the power available at the plane of the satellite. It includes losses due to beam divergence and beam wander. The static losses identified in Table 2 are then added to this main component to yield the total (uplink) loss at the satellite.

Power scintillation index (at the GEO satellite): This metric defines the scintillation at the satellite and is calculated as the ratio of the retrieved power vector's variance at the GEO satellite divided by the square of the mean of this power vector, i.e., $\sigma_I^2 = \langle P^2 \rangle / \langle P \rangle^2$.

1st and 0.1th percentiles: This metric is the 1st and 0.1th percentile values taken from the aforementioned power vector distribution retrieved at the GEO satellite.

6. Results and discussion

6.1. Total (uplink) loss

The mean total (uplink) loss for each AO configuration defined in section 4 is plotted as a function of Fried parameter in Fig. 4, where smaller values of r_0 represent stronger turbulence conditions. The results indicate that the simulated AO system within DLR's OGS achieves a consistent 3-5 dB gain in strong to weak turbulence conditions by applying tip/tilt pre-distortion AO, as compared to not pre-distorting the uplink laser beam. An additional 2-5 dB gain, or 5-10 dB total gain compared to not applying pre-distortion, can be achieved by applying high-order pre-distortion to the uplink laser beam—especially during moderate to strong turbulence conditions. For the realistic tip/tilt and high-order pre-distortion AO configurations, the effect of the point-ahead angle, and thus the potential gain of implementing a laser guide star in the bidirectional FSOC link, does not seem to be considerable—with a potential improvement of only 0.5-1 dB. However, further considerations regarding this will be discussed below. Ultimately, Fig. 4 suggests that the application of pre-distortion AO can significantly improve the mean intensity received at the satellite, which leads to a reduction of the mean total (uplink) losses and an improvement in the overall link budget for the bidirectional FSOC link.

6.2. Power scintillation index

The power scintillation index (PSI) at the GEO satellite for the AO configurations introduced in section 4 is plotted as a function of Fried parameter, r_0, in Fig. 5. This figure is particularly useful as it quantifies the variability in received power at the satellite and the overall link robustness. In weaker turbulence conditions, it is evident that the application of tip/tilt pre-distortion AO significantly reduces the scintillation experienced at the satellite, by roughly a factor of 8, which suggests greatly improved link robustness. When applying high-order pre-distortion AO, the scintillation is reduced by an order of magnitude, as compared to not applying pre-distortion AO. This reduction in scintillation from the high-order pre-distortion AO is maintained as the turbulence strength increases, while the performance due to the application of tip/tilt pre-distortion AO starts to diminish. As with the mean total (uplink) loss from Fig. 4, the link robustness also begins to fail under the strongest of turbulence conditions, as the PSI values drastically increase. It is also important to note the improvement that can be realized by employing a laser guide star in stronger turbulence conditions—even though PSI values greater than 0.4 are still significant. Ultimately, Fig. 5 suggests that applying pre-distortion AO in DLR's next-generation OGS can significantly reduce the scintillation at the satellite, which leads to improved overall link robustness for GEO feeder links.

Optics EXPRESS

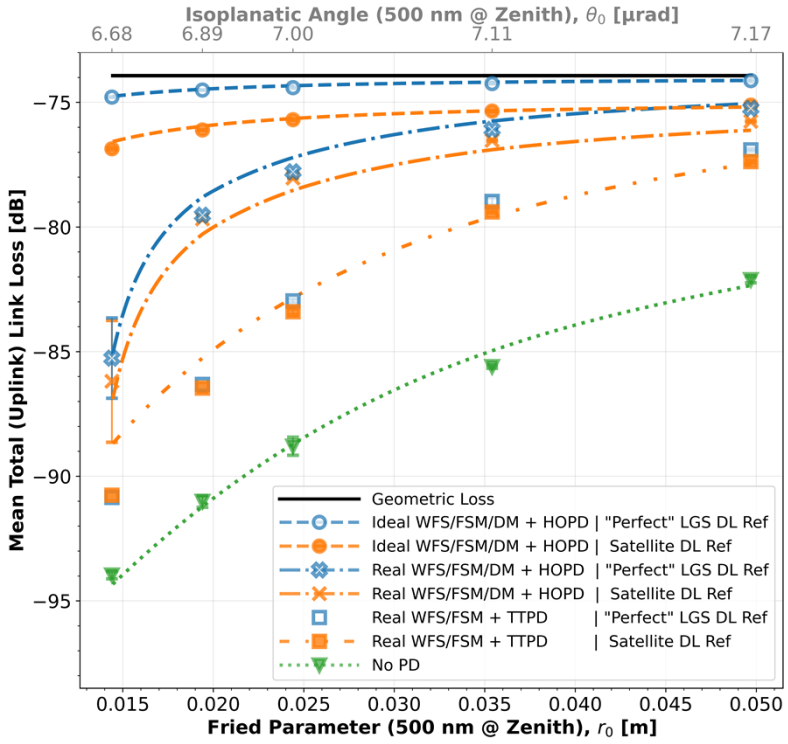

Fig. 4. Mean total (uplink) loss versus Fried parameter, r_0, on the lower horizontal axis and isoplanatic angle on the upper horizontal axis (at zenith and a wavelength of 500 nm). Simulated results are denoted by differing marker shapes and theoretically computed results are denoted by differing line styles. The results are shown for all four configurations introduced in section 4, with blue and orange data representing the first and second sub-configurations, respectively. All simulated results are plotted as the mean of three independent runs of five seconds worth of comparative real-world data, and error bars (when visible) denote the standard error from these three runs.

It is worth noting that the findings presented in Figs. 4 and 5 corroborate the AO error budget from Fig. 3 in that strengthening turbulence conditions, with increasingly fine turbulence structures, can eventually exceed the resolution of the DM and limit the performance of the AO system. Furthermore, the strong scintillation that arises from strong turbulence conditions can cause phase branch points to develop, which degrades the Shack-Hartmann WFS's performance through increasing its measurement error [41]. Concurrently, Figs. 4 and 5 do not show substantial effects due to anisoplanatic or temporal error. Thus, these results suggest that future implementations of pre-distortion AO systems within DLR's OGS (and within other OGS locations that experience similar turbulence conditions) should seek DMs with higher resolution. Wavefront sensors that are more robust in strong turbulence conditions (such as interferometric sensors [31]) could also be further investigated. This can greatly improve the link performance under stronger turbulence conditions, and such improvements can help reduce the disparity seen in Figs. 4 and 5 between the idealized best-case configuration and the realistic high-order and tip/tilt pre-distortion configurations.

Optics EXPRESS

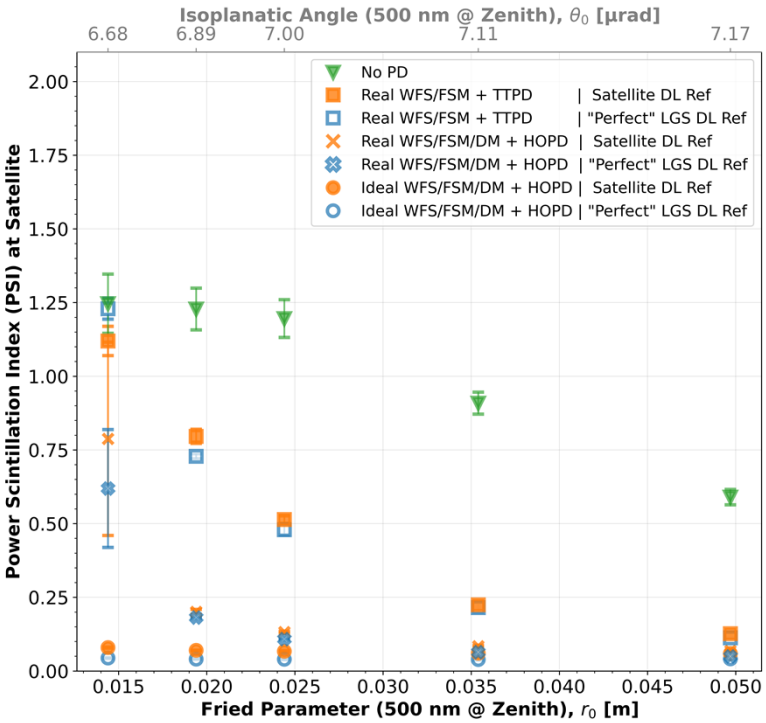

Fig. 5. Power scintillation index (PSI) versus Fried parameter, r_0, on the lower horizontal axis and isoplanatic angle on the upper horizontal axis (at zenith and a wavelength of 500 nm). Simulated results are denoted by differing marker shapes. The results are shown for the four configurations introduced in section 4, with blue and orange data representing the first and second sub-configurations, respectively. All simulated results are plotted as the mean of three independent runs of five seconds worth of comparative real-world data, and error bars (when visible) denote the standard error from these three runs.

6.3. *Considerations for geostationary orbit (GEO) feeder links*

In the context of GEO feeder links serving a large geographical region, such as Europe, it is vital to maximize the link operability. In fact, it is likely that better than 99.9% link uptime must be maintained over weak (nighttime) through strong (daytime) turbulence conditions [9]. With this in mind, we consider the probability density functions (PDF) and cumulative density functions (CDF) for our three strongest turbulence conditions, corresponding to the smallest three values of Fried parameter, r_0. The two remaining r_0 values are not considered, as they do not drastically restrict the link operability. The PDF and CDF results are shown in Fig. 6 as a function of the total (uplink) loss.

The results presented in Fig. 6 corroborate the conclusions made from Figs. 4 and 5, in that greater values of mean power coupled into the satellite are achieved with the application of increasing orders of pre-distortion AO, even in stronger turbulence scenarios. This manifests as a reduction in the total (uplink) losses. Furthermore, the variability of the power received at the GEO satellite is reduced, manifesting as more concentrated PDF distributions and steeper CDF curves in comparison to the broader distributions from no pre-distortion AO being applied.

To evaluate the operability thresholds of GEO feeder links that employ the envisioned bidirectional FSOC link, the 1st and 0.1th percentiles (corresponding to the 99% and 99.9% uptime thresholds, respectively) are extracted from Fig. 6 and are plotted in Fig. 7 as a function of

Optics EXPRESS

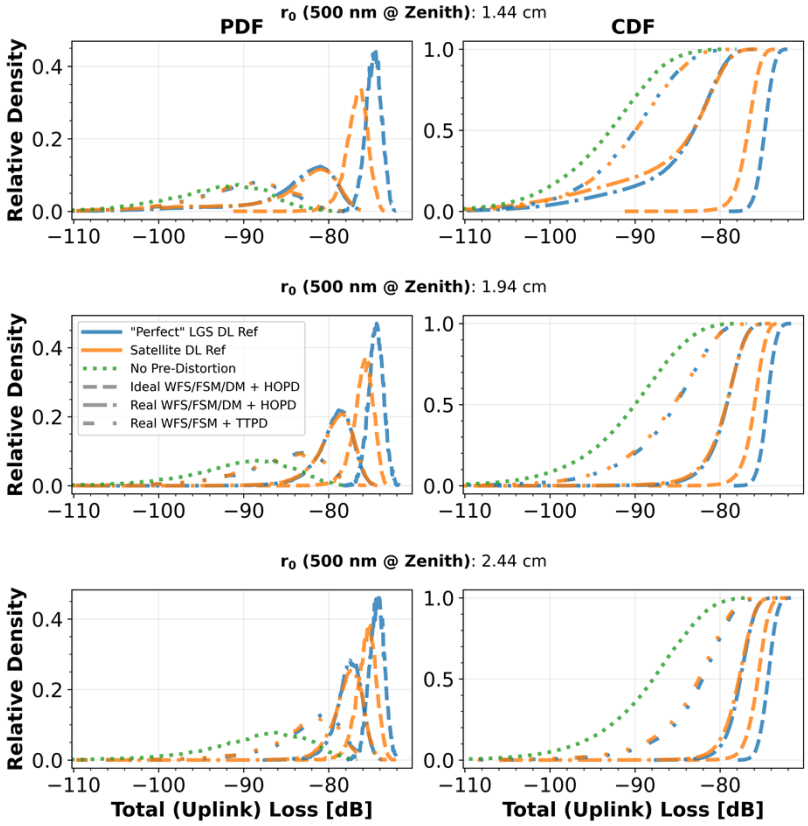

Fig. 6. Probability density functions (PDF) and cumulative density functions (CDF) versus total (uplink) loss for our three strongest turbulence conditions, i.e., the three smallest values of Fried parameter, r_0. The results are shown for the four AO configurations and two sub-configurations introduced in section 4. The *dashed*, *dot-dashed*, *dot-dot-dashed*, and *dotted* lines correspond to the *first*, *second*, *third*, and *fourth* configurations, respectively. The blue and orange curves depict the first and second sub-configurations, respectively. The distributions presented in this figure are made from the prior simulated datapoints, and are not theoretically calculated curves.

increasing values of Fried parameter, r_0. Note that the lines joining the simulated data points in Fig. 7 are added for readability and do not represent the theoretical models introduced in section 3.

Figure 7 demonstrates the challenge of maintaining near continuous operation of GEO feeder links and the notable benefits from pre-distortion AO. Under weak turbulence conditions, the results suggest that for the 1st and 0.1th percentiles, tip/tilt pre-distortion AO significantly reduces the total (uplink) loss and yields immense gains, at approximately 20-40 dB. As the turbulence conditions worsen, these gains can be maintained by applying higher-order pre-distortion. This is understandable given that stronger turbulence demands greater spatial resolution in the AO system. It is also clear that fitting error limits the performance as the realistic pre-distortion AO configuration results rapidly depart from the idealized configuration results during strong turbulence conditions.

Another noteworthy aspect of the results presented in Fig. 7 is the effect of anisoplanatism, and thus the potential performance gains of using a laser guide star. Even in moderate to weak turbulence, anisoplanatic effects can yield fairly significant losses. Therefore, assuming a GEO

Optics EXPRESS

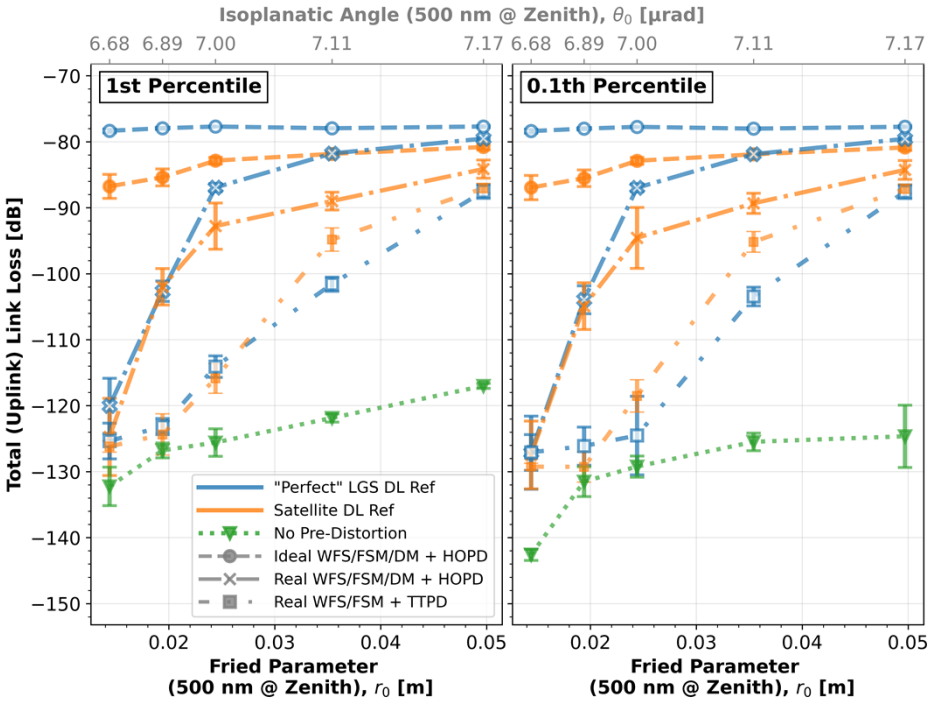

Fig. 7. The 1st and 0.1th percentile values extracted from Fig. 6 and plotted as a function of increasing values of Fried parameter, r_0, corresponding to decreasing turbulence strength. The simulated results denoted by *circles*, *crosses*, *squares*, and inverted *triangles* correspond to the *first*, *second*, *third*, and *fourth* configurations from section 4, respectively. The *blue* and *orange* simulated markers represent the *first* and *second* sub-configurations from section 4, respectively. All data shown in this figure is derived from simulated results. The lines joining adjacent data points are added for readability and do not represent theoretical analyses from prior sections.

feeder link scenario requires 99.9% uptime, the results suggest that a maximum potential gain of 7-8 dB could be realized by employing a laser guide star in moderately strong turbulence conditions. This significantly reduces the total (uplink) loss and thus the threshold for near continuous link operation. Such a finding demonstrates the importance of analyzing percentiles as a figure of merit, as the reduction by the idealized laser guide star was not apparent in Figs. 4 and 5. While the laser guide star used in this work is admittedly idealized, given the impressive gains that can be realized by realistic pre-distortion AO, it is plausible to expect sustained improvements from realistic laser guide stars in moderate to strong turbulence conditions. Ultimately, the application of a laser guide star significantly reduces the variability of power received at the GEO satellite and eases the performance demands to maintain 99.9% link operability of the bidirectional FSOC link for a GEO feeder link scenario.

7. Conclusion

This work presented performance analyses of a bidirectional FSOC link between DLR's next-generation OGS, employing pre-distortion AO, and the GEO satellite Alphasat. The analyses were performed by way of realistic end-to-end Monte Carlo simulations that incorporated real-world errors for the link and AO system. It was found that applying tip/tilt pre-distortion could mitigate much of the mean total (uplink) losses, by 3-5 dB, as compared to not applying pre-distortion

Optics EXPRESS

AO. An additional 3-5 dB, or 5-10 dB total improvement, could also be realized by applying high-order pre-distortion AO (and particularly under strong turbulence conditions). The power scintillation index was also found to be significantly reduced, by approximately an order of magnitude, through the application of high-order pre-distortion in weak to moderate turbulence conditions. This suggests notable improvements for the robustness of GEO feeder links. The performance estimates for the pre-distortion AO system within DLR's next generation OGS were found to be dominated by fitting wavefront error, and so future pre-distortion AO systems (operating in similar turbulence conditions) may wish to operate with higher resolution DMs. Furthermore, wavefront sensing solutions that perform better than a Shack-Hartmann type WFS in strong turbulence conditions could also be explored.

When considering the needs for near continuous link operation, at 99.9% uptime for the bidirectional FSOC link in a GEO feeder link scenario, it was found that applying pre-distortion AO could yield significant improvements in the total (uplink) loss, by 20-40 dB, even in strong turbulence conditions. The employment of a laser guide star could then further reduce the total (uplink) loss, with our idealized case showing a reduction of 8 dB. Ultimately, we hope that these findings will lay the groundwork for refined FSOC technology and improved performance in future GEO feeder links.

Funding. Bayerisches Staatsministerium für Wirtschaft und Medien, Energie und Technologie (LABAY98C); DLR-DAAD Doctoral Research Fellowship (57540125); Natural Sciences and Engineering Research Council of Canada (RGPIN-2017-0407); UK Research and Innovation (MR/X015106/1).

Acknowledgments. The in-house simulation used within this work employs the following Python packages: NumPy [42], Scipy [43], AOtools [44], and Matplotlib [45]. The authors also wish to thank Andrea Carrillo Flores for her technical input.

Disclosures. The authors declare no conflicts of interest.

Data availability. Data underlying the results presented in this paper are not publicly available at this time but may be obtained from the authors upon reasonable request.

References

1. Canadian Space Agency, *Exploration Imagination Innovation: A new space strategy for Canada* (CSA Public Report, 2020).
2. European Space Agency, *ESA specification for terabit/sec optical links (ESTOL)* (ESA Public Report, 2023).
3. E. Agrell, M. Karlsson, A. R. Chraplyvy, *et al.*, "Roadmap of optical communications," J. Opt. **18**(6), 063002 (2016).
4. Z. Sodnik, C. Voland, J. Perdigues, *et al.*, "Optical feeder-link between ESA's optical ground station and Alphasat," in *SPIE 11852, International Conference on Space Optics—ICSO 2020, 1185218* (2021), pp. 1–7.
5. R. Mata Calvo, T. de Cola, J. Poliak, *et al.*, "Optical feeder links for future very high-throughput satellite systems in B5 G networks," in *2020 European Conference on Optical Communications (ECOC)* (2020), pp. 1–4.
6. R. Barrios, S. Dimitrov, R. Mata-Calvo, *et al.*, "Link budget assessment for GEO feeder links based on optical technology," Int. J. Satell. Commun. Network. **39**(2), 160–177 (2021).
7. C. Fuchs, D. Giggenbach, R. Mata Calvo, *et al.*, "Transmitter diversity with phase-division applied to optical GEO feeder links," IEEE Photonics Technol. Lett. **33**(11), 541–544 (2021).
8. W. Cowley, D. Giggenbach, R. Mata Calvo, *et al.*, "Optical transmission schemes for GEO feeder links," in *2014 IEEE International Conference on Communications (ICC)* (2014), pp. 4154–4159.
9. C. Fuchs, S. Poulenard, N. Perlot, *et al.*, "Optimization and throughput estimation of optical ground networks for LEO-downlinks, GEO-feeder links and GEO-relays," in *SPIE 10096, Free-Space Laser Communication and Atmospheric Propagation XXIX* (2017), pp. 1–10.
10. R. Mata Calvo, J. Poliak, J. Surof, *et al.*, "Optical technologies for very high throughput satellite communications," in *SPIE 10910, Free-Space Laser Communications XXXI*, 109100W (2019), pp. 1–4.
11. L. C. Andrews and R. L. Phillips, *Laser beam propagation through random media*, 2nd ed. (SPIE—The International Society for Optical Engineering, 2005).
12. A. K. Majumdar and J. C. Ricklin, *Free-space laser communications: principles and advances* (Springer Science & Business Media, 2008).
13. X. Zhu and J. Kahn, "Free-space optical communication through atmospheric turbulence channels," IEEE Trans. Commun. **50**(8), 1293–1300 (2002).
14. R. K. Tyson, "Adaptive optics and ground-to-space laser communications," Appl. Opt. **35**(19), 3640–3646 (1996).
15. J. Cao, X. Zhao, W. Liu, *et al.*, "Performance analysis of a coherent free space optical communication system based on experiment," Opt. Express **25**(13), 15299–15312 (2017).

Optics EXPRESS

16. Y. Wang, H. Xu, D. Li, *et al.*, "Performance analysis of an adaptive optics system for free-space optics communication through atmospheric turbulence," Sci. Rep. **8**(1), 1124 (2018).
17. J. Osborn, M. J. Townson, O. J. D. Farley, *et al.*, "Adaptive optics pre-compensated laser uplink to LEO and GEO," Opt. Express **29**(4), 6113–6132 (2021).
18. S. Dimitrov, R. Barrios, B. Matuz, *et al.*, "Digital modulation and coding for satellite optical feeder links with pre-distortion adaptive optics," Int. J. Satell. Commun. Network. **34**(5), 625–644 (2016).
19. N. Martínez, L. F. Rodríguez-Ramos, and Z. Sodnik, "Toward the uplink correction: application of adaptive optics techniques on free-space optical communications through the atmosphere," Opt. Eng. **57**(07), 1 (2018).
20. N. Védrenne, A. Montmerle-Bonnefois, C. B. Lim, *et al.*, "First experimental demonstration of adaptive optics pre-compensation for GEO feeder links in a relevant environment," in *2019 IEEE International Conference on Space Optical Systems and Applications (ICSOS)*, (2019), pp. 1–5.
21. T. von Kármán, "The fundamentals of the statistical theory of turbulence," J. Aeronaut. Sci. **4**(4), 131–138 (1937).
22. T. von Kármán, "Progress in the statistical theory of turbulence," Proc. Natl. Acad. Sci. U.S.A. **34**(11), 530–539 (1948).
23. J. D. Schmidt, *Numerical simulation of optical wave propagation with examples in MATLAB* (SPIE—The International Society for Optical Engineering, 2010).
24. J. W. Hardy, *Adaptive Optics for Astronomical Telescopes* (Oxford University Press Inc., 1998).
25. K. Saucke, J. Woicke, R. Mahn, *et al.*, "Characterisation of the optical channel GEO to ground: using five years of data from Alphasat TDP1 and T-AOGS for investigation of different conditions," in *SPIE 11852, International Conference on Space Optics—ICSO 2020, 118525W* (2021), pp. 1–13.
26. J. L. Bufton, "Comparison of vertical profile turbulence structure with stellar observations," Appl. Opt. **12**(8), 1785–1793 (1973).
27. T. Fusco, J.-M. Conan, V. Michau, *et al.*, "Efficient phase estimation for large-field-of-view adaptive optics," Opt. Lett. **24**(21), 1472–1474 (1999).
28. R. Griffiths, J. Osborn, O. Farley, *et al.*, "Demonstrating 24-hour continuous vertical monitoring of atmospheric optical turbulence," Opt. Express **31**(4), 6730–6740 (2023).
29. D. J. Laidlaw, A. P. Reeves, H. Singhal, *et al.*, "Characterizing turbulence profile layers through celestial single-source observations," Appl. Opt. **61**(2), 498–504 (2022).
30. L. Westerby-Griffin, J. Osborn, O. J. D. Farley, *et al.*, "Atmospheric optical turbulence analysis in London's financial district," in *SPIE 12413, Free-Space Laser Communications XXXV*, 124131F (2023), pp. 1–4.
31. R. K. Tyson, *Principles of Adaptive Optics* (Academic Press Inc., 1991).
32. R. Hudgin, "Wave-front compensation error due to finite corrector-element size," J. Opt. Soc. Am. **67**(3), 393–395 (1977).
33. Y. Clénet, E. Gendron, D. Gratadour, *et al.*, "Anisoplanatism effect on the E-ELT SCAO point spread function. A preserved coherent core across the field," Astron. Astrophys. **583**, A102 (2015).
34. F. Chassat, "Theoretical evaluation of the isoplanatic patch of an adaptive optics system working through the atmospheric turbulence," J. Opt. **20**(1), 13–23 (1989).
35. P. Lognoné, J.-M. Conan, G. Rekaya, *et al.*, "Phase estimation at the point-ahead angle for AO pre-compensated ground to GEO satellite telecoms," Opt. Express **31**(3), 3441–3458 (2023).
36. L. C. Andrews, R. L. Phillips, R. J. Sasiela, *et al.*, "Strehl ratio and scintillation theory for uplink Gaussian-beam waves: beam wander effects," Opt. Eng. **45**(7), 076001 (2006).
37. A. Maréchal, "Étude des effets combinés de la diffraction et des aberrations géometriques sur l'image d'un point lumineux," Rev. d'Opt. **26**, 257–277 (1947).
38. V. N. Mahajan, "Strehl ratio for primary aberrations: some analytical results for circular and annular pupils," J. Opt. Soc. Am. **72**(9), 1258–1266 (1982).
39. V. N. Mahajan, "Strehl ratio of a Gaussian beam," J. Opt. Soc. Am. A **22**(9), 1824–1833 (2005).
40. T. S. Ross, "Limitations and applicability of the Maréchal approximation," Appl. Opt. **48**(10), 1812–1818 (2009).
41. J. D. Barchers, D. L. Fried, and D. J. Link, "Evaluation of the performance of Hartmann sensors in strong scintillation," Appl. Opt. **41**(6), 1012 (2002).
42. S. Van der walt, S. C Colbert, and V. Gaël, "The NumPy array: a structure for efficient numerical computation," Comput. Sci. Eng. **13**(2), 22–30 (2011).
43. P. Virtanen, R. Gommers, T. E. Oliphant, *et al.*, "SciPy 1.0: fundamental algorithms for scientific computing in Python," Nat. Methods **17**(3), 261–272 (2020).
44. M. J. Townson, O. J. D. Farley, G. Orban de Xivry, *et al.*, "AOtools: a Python package for adaptive optics modelling and analysis," Opt. Express **27**(22), 31316 (2019).
45. J. D. Hunter, "Matplotlib: A 2D graphics environment," Comput. Sci. Eng. **9**(3), 90–95 (2007).